Catalysis Science & Technology

Accepted Manuscript

ROYAL SOCIETY OF CHEMISTRY

www.rsc.org/catalysis

Activated-carbon-supported K–Co–Mo catalyst for synthesis of higher alcohols from syngas

Meimei Lv[a], Wei Xie[a], Song Sun[a*], Gaimei Wu[a], Lirong Zheng[b], Shengqi Chu[b], Chen Gao[a,c], Jun Bao[a,c*]

[a] National Synchrotron Radiation Laboratory, Collaborative Innovation Center of Chemistry for Energy Materials, University of Science & Technology of China, Hefei, Anhui, 230029, China

[b] Institute of High Energy Physics, Chinese Academy of Science, Beijing, 100039, China

[c] CAS Key Laboratory of Materials for Energy Conversion, Department of Materials Science and Engineering, University of Science & Technology of China,
Hefei, Anhui, 230026, China

[*]Corresponding author. Fax: (+86) 551-6514-1078; Tel: (+86) 551-6360-7492;
E-mail: baoj@ustc.edu.cn; suns@ustc.edu.cn

Abstract

A series of activated-carbon-supported K–Co–Mo catalysts (K–Co–Mo/AC) were prepared by a sol–gel method combined with incipient wetness impregnation. The catalyst structure was characterized by X-ray diffraction (XRD), N_2 adsorption–desorption, and X-ray absorption fine structure and X-ray photoelectron spectroscopy techniques, and its catalytic performance toward the synthesis of higher alcohols from syngas was investigated. The large surface area and pore volume of the support facilitated the distribution of metal particles and high dispersion of metals. At low Mo loading, the Mo atoms on the activated carbon surface were mainly tetrahedral-coordinated Mo^{6+} species. With an increase in the Mo loading, the coordination environment of the surface Mo atoms gradually transformed from tetrahedrally coordinated Mo^{6+} to octahedrally coordinated Mo^{4+}, indicating that an increase in the Mo loading promoted the reduction of Mo^{6+} to Mo^{4+} species. After reduction, a type of a lower state $Mo^{\delta+}$ ($1 < \delta < 4$) species was present on the surface, which is suggested to be responsible for alcohol synthesis. Compared to the unsupported catalyst, K–Co–Mo/AC exhibited a significantly higher activity for alcohol formation. In particular, C_{2+} alcohol content increased significantly. The reason can be attributed to the fact that the supported catalyst has a high active surface area, and the mesoporous structure is suggested to prolong the residence time of intermediates to form alcohols in the pore to some extent, thus promoting the formation of higher alcohols. Under condition of a Mo/AC weight ratio of 40% and reduction temperature of 798 K, the catalyst exhibited the highest activity for alcohol

formation, which may be attributed to the high content of $Mo^{\delta+}$ ($1 < \delta < 4$) species on the surface.

Keywords: Higher alcohol synthesis; Activated carbon support; XAFS; K–Co–Mo catalyst

1 Introduction

In the last few decades, the synthesis of higher alcohols by the catalytic conversion of syngas has attracted significant attention because of scarcity of energy resources as well as an increase in environmental pollution and gasoline additive octane demands. Moreover, as gasoline boosters, higher alcohols are preferred over widely used methanol because of their lower volatility, higher solubility in hydrocarbons, and higher calorific value. Typically, among the catalysts studies for the synthesis of higher alcohols[1], Mo-based catalysts are most promising as they exhibit high resistance to sulfur poisoning and deactivation by coking.[2] The addition of an alkali to a Mo-based catalyst increases alcohol formation and suppresses hydrocarbon formation.[3]

Some 3d transition metals, especially Co, are found to be effective promoters for alkali-promoted Mo-based catalysts; they are known to enhance alcohol production; in particular, they improve C_{2+} alcohol selectivity. Xiang et al.[4] have reported that transition metal (Fe, Co, Ni)-modified K/Mo_2C catalysts exhibit a sharp increase in both the activity and selectivity for $C_{2+}OH$. For MoS_2-based catalysts, the addition of Co, Ni, Rh, and Pd are favorable for improving catalytic performance and higher alcohol selectivity.[5] The incorporation of Co resulted in substantial changes in the

structure of K-modified MoS_2 catalysts and promoted chain growth, which leads to $C_{2+}OH$ formation. [6] The Co species operated as a synergistic system with the MoS_2 phase, rather than independently from the MoS_2 phase.[7] Surisetty et al.[6] have demonstrated that the addition of Co to K–MoS_2/multiwalled carbon nanotube catalyst not only increases the number of surface molybdenum sites but also promotes the reduction of molybdenum, which in turn enhances the total alcohol space time yield (STY) and the selectivity for ethanol. Similarly, over the reduced K–Mo/Al_2O_3 and K–Mo/SiO_2 catalysts, the addition of Co also increases the activity toward the formation of higher alcohols, caused by the strong interaction between the Co promoter and the Mo species.[8]

Catalyst supports significantly affect the synthesis of alcohols from syngas. Dadyburjor et al. have suggested that the addition of a support with a K-promoted Co–Mo sulfide catalyst results in an increase in the yields of both alcohols and hydrocarbons, on a Mo basis.[9] Different catalyst supports for Mo catalysts have been investigated in literature.[3c, 5c, 10] Some acid metal oxide supports such as Al_2O_3 and SiO_2 are unfavorable to form alcohols because of the alcohol dehydration on the acidic sites of supports and catalyst deactivation by coke formation.[11] Activated carbon supports have some potential advantages such as large surface area, high thermal stability, resistance to acidic or basic media, low tendencies of carbon deposition, and less dehydration.[12] Alcohol selectivity is observed to be higher with the use of an activated-carbon-supported Mo-based catalyst as compared to SiO_2-, Al_2O_3-, and CeO_2-supported catalysts.[12-13] The interaction between Mo species and

the activated carbon support has a noticeable effect on the reduction behavior of the catalysts.

In our previous study, a highly homogeneous and dispersed K–Co–Mo catalyst was prepared by a sol–gel method, which exhibits high alcohol yield, especially high selectivity for $C_{2+}OH$, for the synthesis of higher alcohols from syngas.[14] However, its characteristics of large pore size, very small surface area, and pore volume are not conducive for synthesizing alcohols. To further improve the catalytic activity and understand the relationship between the properties of supports and catalytic performance, in this study, mesoporous activated carbon was incorporated as the support to prepare the K–Co–Mo/AC catalysts by a sol–gel method combined with incipient wetness impregnation. The activity of the catalyst for the synthesis of higher alcohols from syngas was investigated, and its structure was characterized by X-ray diffraction (XRD), N_2 physisorption, X-ray absorption fine structure (XAFS), and X-ray photoelectron spectroscopy (XPS). The relationship between the structure and catalytic performance was also discussed.

2 Experimental

2.1 Catalyst Preparation

Activated carbon (AC)-supported K–Co–Mo catalysts were prepared by a sol–gel method combined with incipient wetness impregnation. Activated carbon was supplied by FUJIAN XINSEN CARBON CO. LTD. $(NH_4)_6Mo_7O_2{\cdot}4H_2O$ (99.0%), $Co(NO_3)_2{\cdot}6H_2O$ (99.0%), $C_6H_8O_7{\cdot}H_2O$ (99.5%), and K_2CO_3 (99.0%) were supplied by SINOPHARM CHEMICAL REAGENT CO., LTD. The K–Co–Mo sol was

prepared, as described in our previous study.[15] The as-prepared sol was then impregnated into activated carbon. After ultrasonic dispersion for 5 min, the mixture was dried at 393 K overnight and calcined in flowing nitrogen at 673 K for 4 h. The atomic ratios of K/Mo and Co/Mo were 0.1 and 0.5, respectively. The Mo content in the samples, expressed as the Mo/AC weight ratio, ranged from 10% to 50%. The size of the activated carbon particles is 10–20 mesh. Before use, the support was first washed using 30% nitric acid and deionized water, followed by drying in air at 393 K overnight and then flushing with nitrogen (99.999%) at 453 K for 2 h to remove any surface adsorbents.

2.2 Catalyst Characterization

The Brunauer–Emmett–Teller (BET) surface area was determined by nitrogen adsorption at 77 K using a Micromeritics TriStar II 3020 analyzer. For each analysis, approximately 0.1 g of sample was used. Powder XRD patterns were obtained on a Rigaku D/max-γA rotating-anode diffractometer equipped with a Cu Kα radiation source at 40 kV and 200 mA with a scan range of 10–70°. The surface chemical composition of the catalyst was analyzed by XPS (Thermo ESCALAB 250) using Al Kα ($h\nu$ = 1486.6 eV) as the X-ray source. The binding energy of C1s (284.5 eV) was used as a reference to correct the binding energy of the catalysts. Baseline correction was conducted by the Shirley method. Mo $3d_{5/2}$ and Mo $3d_{3/2}$ peaks were separated by 3.15 eV with peak ratios of 3/2. All binding energies obtained in this study were precise to within ±0.2 eV.

The Mo K-edge XAFS spectral measurements were performed on beam-line of 4W1B at the Beijing Synchrotron Radiation Facility. The storage ring energy was 2.5 GeV with an average current of 80 mA. Spectra were obtained in the transmission mode using a Si(111) double-crystal monochromator. The energy calibration of Mo K-edge was performed using a Mo foil. All samples were ground and sieved through 400 mesh and brushed onto tapes that were stacked together to give approximately one X-ray absorption length at the Mo K-edge. Data processing was conducted by the standard procedure of background absorption removal and normalization.

2.3 Catalytic Activity Measurement

The catalytic activity for the synthesis of higher alcohols from CO hydrogenation was measured in a fixed-bed stainless steel reactor with an inner diameter of 8 mm. First, 0.5 g of catalyst was loaded at the center of the reactor tube, which was diluted with quartz sand to make a total volume of 2 ml. Prior to the reaction, the catalyst was reduced in a mixed flow of H_2/N_2 (5 vol% H_2) at a flow rate of 40 ml/min for 12 h. Second, the temperature of the reactor was lowered to the reaction temperature, and syngas containing 30% CO, 60% H_2, and 10% N_2 was introduced into the reactor. Third, the effluent gas was cooled in an ice-water bath to separate into gas and liquid phases at the reaction pressure. CO, CO_2, CH_4, and N_2 were directly analyzed using an on-line gas chromatograph (KEXIAO, GC-1690, thermal conductivity detector) equipped with a 3 m TDX-01 packed column through a sampling valve. High-purity H_2 was used as the carrier gas. Gaseous hydrocarbons were directly analyzed by an

on-line gas chromatograph (KEXIAO, GC-1690, flame ionization detector (FID)) equipped with a 3 m Porapak Q packed column through a sampling valve with N_2 as the carrier gas. Liquid products were also analyzed on the same FID chromatograph by injection after collection for an appropriate period. The hydrocarbon concentration was calculated using 99.99% CH_4 as the standard gas, and the mixed alcohol was directly calculated from the peak area by using a standard liquid of mixed alcohol. H_2O contents in liquid products were analyzed using a moisture meter (ANTING, ZSD-2). Because the synthesis of higher alcohols requires an induction period to reach a steady-state condition, all activity data shown in this study were measured after the reaction was performed for more than 24 h.

3 Results and discussion

3.1 XRD Results

Figure 1 shows the XRD patterns of fresh K–Co–Mo/AC catalysts at different weight ratios of Mo/AC. For comparison, the diffraction patterns of the activated carbon support and unsupported K–Co–Mo catalyst are also listed. Activated carbon exhibited two weak and wide diffraction peaks. For the unsupported catalyst, three peaks were observed at 26.1°, 37.0°, and 53.5°, which correspond to MoO_2. Besides these peaks, no peaks assigned to K–Mo or Co species were detected. MoO_2 formation can be attributed to the fact that in nitrogen, the decomposition of citric acid in the precursor sol partly reduced the Mo^{+6} species.[15] The activated-carbon-supported K–Co–Mo catalysts exhibited significantly weaker diffraction intensity than the sole support or unsupported catalyst. For the catalysts

with Mo/AC weight ratio of 30% and 40%, the very weak peaks at about 26.7°, 28.5° and 33.6° may be assigned to $CoMoO_4$ species. Almost no clear peaks were observed when the Mo/AC weight ratio exceeded 50%. After reduction at 773 K, only very weak diffraction peaks of MoO_2 species were observed (Figure 2). The results indicate that for the supported K–Co–Mo/AC catalysts, the active components exhibit high dispersion on the activated carbon surface.

3.2 Nitrogen Adsorption–Desorption Results

Figure 3 shows the nitrogen adsorption–desorption isotherms of activated carbon and the K–Co–Mo/AC and unsupported K–Co–Mo catalyst. The activated carbon support exhibited a type I isotherm with a hysteresis loop of type H4 according to the IUPAC classification.[16] Capillary condensation in pores occurred at a relative pressure (p/p_o) above 0.40. This indicates the presence of a large amount of narrow slit-like mesopores. The unsupported K–Co–Mo catalyst exhibited a characteristic type III isotherm with a hysteresis loop of type H3, which did not exhibit any limiting adsorption at high relative pressures. Furthermore, the condensation of adsorbates in the pores occurred at a relative pressure higher than that of activated carbon and supported catalysts, indicative of a larger pore size. This H3 type of a hysteresis loop is usually observed for solids consisting of agglomerates of particles forming conical-shaped pores with a non-uniform size. Figure 3b–e shows nitrogen adsorption–desorption isotherms of the activated-carbon-supported K–Co–Mo catalysts with different Mo loading. From the figures, all the supported catalysts

exhibited isotherms similar to that exhibited by activated carbon, suggesting that metal impregnation did not alter the pore structure of the parent support. Table 1 lists the textural properties of the pure support as well as the supported and unsupported catalysts. The activated carbon support had a high BET surface area, large pore volume, and mesoporous structure. By contrast, the unsupported K–Co–Mo catalyst had a very small surface area and total pore volume compared with those of the activated carbon and supported catalysts. On the other hand, its pore diameter was quite large. The activated-carbon-supported K–Co–Mo catalysts exhibited some changes as compared to the pure support. The BET surface area and pore volume decreased after the impregnation of alkali and metals on the support, suggesting that the partial pores of the support are blocked by the metals. The average pore diameter was shifted toward higher values after metal incorporation. The results suggest that the addition of metals most likely block the micropores of the support. Despite pore blockage, the mesoporous structural integrity of the supported catalysts was unchanged from the activated carbon support, as can be observed from the nitrogen adsorption–desorption isotherms of the pure support and supported catalyst.

3.3 XAFS Results

Figure 4 shows the Mo K-edge X-ray absorption near-edge structure (XANES) spectra of the K–Co–Mo/AC catalysts together with those of the unsupported sample and standard compounds MoO_2 and MoO_3. XANES spectra can provide detailed information about the oxidation state and coordination environment of the metal

atoms. The absorption edge energy can be used to determine chemical valence; the edge energy increased with increasing oxidation state. The pre-edge feature reflected a 1s→4d electronic transition, which is a dipole-forbidden transition for structures having an inversion center. The pre-edge peak intensity was sensitive to the symmetry of the absorbing atom and can provide structural information about the first coordination shell. The compounds in which the absorbing atom was tetrahedrally coordinated generally exhibited intense pre-edge peaks. In the case of octahedrally coordinated compounds, such pre-edge peaks were usually weak. MoO_3 is composed of layers of distorted MoO_6 octahedra in an orthorhombic crystal. Each molybdenum atom is coordinated by six oxygen atoms with Mo–O distances ranging from 1.67 to 2.33 Å.[17] The Mo^{6+} cations in MoO_3 occupy off-center positions in distorted MoO_6 octahedra, and this distortion allows the 1s→4d electronic transition to occur. As a result, a weak pre-edge peak was observed in the XANES spectra of MoO_3, as shown in Figure 4. MoO_2 crystallizes in a monoclinic cell and exhibits a distorted rutile structure, in which each metal atom is surrounded by six oxygen atoms, while each oxygen atom is surrounded by three metal atoms at the corners of an equilateral triangle.[17] Compared to MoO_3, MoO_2 has a strictly octahedral field. The 1s→4d transition is forbidden in octahedral symmetry; consequently, no pre-edge peak was evident in this spectrum.

For the unsupported K–Co–Mo catalyst, a weak pre-edge peak was observed, and the absorption edge was close to that of MoO_3, indicating the presence of octahedral Mo^{6+} species. The supported K–Co–Mo/AC catalyst with a Mo/AC weight ratio of

10% exhibited an intense pre-edge peak, and the absorption edge was consistent with that of MoO_3. With an increase in the Mo loading, the pre-edge peak became weaker, and the absorption edge shifted to lower energy, close to that of MoO_2. The results suggest that at low Mo loading, the Mo atoms on the activated carbon surface were mainly tetrahedrally coordinated Mo^{6+} species. With an increase in the Mo loading, the coordination environment of surface Mo atoms gradually transformed from a tetrahedral to octahedral structure, and the percentage of Mo^{4+} species increased, indicating that an increase in the Mo loading can promote the reduction of Mo^{6+} to Mo^{4+} species. Similar results have been reported for Mo/Al_2O_3, where the coordination of the surface molybdenum oxide species on $A1_2O_3$ changes from tetrahedral to octahedral with increasing Mo coverage.

Figure 5 shows the Fourier transforms of Mo K-edge EXAFS of the K–Co–Mo/AC catalysts together with the unsupported sample and standard compounds MoO_2 and MoO_3. The K–Co–Mo/AC with a Mo/AC weight ratio of 10% exhibited intense Mo–O coordination, but almost no Mo–Mo coordination was observed. The result suggests that at a low Mo loading, the Mo species was dispersed as a monolayer on the activated carbon surface. Furthermore, the sample had a lower R value of Mo–O coordination compared with those of MoO_2 and MoO_3, which may be caused by their different coordination environments, as revealed by XANES spectra results. With an increase in the Mo loading, clear Mo–Mo coordination was observed, and the FT exhibited a feature similar to that of MoO_2, indicating the formation of MoO_2 species. The result is consistent with those of XRD and XANES.

The Mo–O coordination shifted to a larger R value and became broader as the Mo loading increased. Meanwhile, a weak shoulder peak attributed to the Mo–O coordination of MoO_2 was observed. The results suggest that at high surface coverage of Mo species, a mixture of tetrahedral- and octahedrally coordinated Mo species exist. The Mo atoms directly connected to the activated carbon surface was tetrahedrally coordinated Mo^{6+}. With an increase in Mo loading, the octahedrally coordinated Mo^{4+} species gradually formed over it.

3.4 XPS Results

Figure 6 shows the XPS spectra of Mo 3d for fresh K–Co–Mo/AC catalysts at different weight ratios of Mo/AC. The distribution of the Mo oxidation state was estimated by the deconvolution of the Mo 3d doublet, which consisted of two peaks as a result of spin–orbit (j–j) coupling. The doublets were fitted so that each peak had the same Gaussian line shape and the same full-width at half-maximum. The splitting energy is known to be approximately 3.15 eV, while the relative area ratios of spin–orbit doublet peaks should be 3/2, following the ratio of their respective degeneracies (2j+1) [18]. The percentage of Mo species with different oxidation states was calculated on the basis of the peak area, and the results are summarized in Table 2. For the catalyst with a Mo/AC weight ratio of 10%, only characteristic binding energies of Mo^{6+} $3d_{5/2}$ (232.5 eV) and Mo^{6+} $3d_{3/2}$ (235.6 eV) were observed. At a higher Mo loading, besides the Mo^{6+} state, two new peaks assigned to Mo^{4+} $3d_{5/2}$ (230.8 eV) and Mo^{4+} $3d_{3/2}$ (234.0 eV) appeared, indicating the formation of Mo^{4+}

species. The percentage of surface of Mo^{4+} species increased with Mo loading, further providing evidence that an increase in the Mo loading can promote the reduction of Mo^{6+} species, as revealed by XANES spectra. After reduction, as shown in Figure 7 and Table 3, two new peaks were observed at 229.4 eV and 232.6 eV, which can be attributed to the binding energies of $Mo^{\delta+}$ ($1 < \delta < 4$) $3d_{5/2}$ and $Mo^{\delta+}$ $3d_{3/2}$, respectively [18]. With an increase in the Mo loading, the percentage of $Mo^{\delta+}$ species achieved the maximum value at the catalyst with a Mo/AC weight ratio of 40%. The Mo^{6+} content decreased, while the Mo^{4+} content did not show any obvious change as the Mo loading increased. It is noted that the binding energies of Mo^{6+} and Mo^{4+} states shifted toward lower levels after reduction. The reason for this shift can be attributed to the fact that H_2 reduction increased the electron cloud density, intensified the electromagnetic shield for the inner shell electron, and consequently decreased the electron binding energy. Figure 8 shows the XPS spectra of Mo 3d for the K–Co–Mo/AC catalysts at different reduction temperatures. The effect of reduction temperature on the Mo oxidation state was also analyzed. As listed in Table 4, for the catalyst with a Mo/AC weight ratio of 40%, the percentage of surface $Mo^{\delta+}$ increased with an increase in the reduction temperature and reached a maximum value at 798 K. With a further increase in the temperature, the $Mo^{\delta+}$ content decreased, which may be attributed to the fact that high temperature resulted in the sintering of particles and in the inhibition of the reduction of Mo species.[15]

3.5 Catalytic Performance

The catalytic performance of the K–Co–Mo/AC catalysts for the synthesis of higher alcohols was tested under the conditions of 573 K, 5.0 MPa, 2400 h^{-1}, and a H_2 to CO molar ratio of 2. Table 5 lists the activity data after an induction period of 24 h. For comparison purposes, the unsupported catalyst was tested under the same conditions. Over the unsupported catalyst, the STY and selectivity toward alcohol synthesis were relative low, and the predominant alcohol product was methanol. When activated carbon was incorporated as a support, catalytic performance was remarkably enhanced. As shown in Table 5, the alcohol STY and selectivity, as well as the $C_{2+}OH$ content in alcohol distribution, significantly increased with an increase in the Mo loading and reached the highest level on the catalyst with a Mo/AC weight ratio of 40%. On the catalyst, the STY of total alcohol was 126.2 $g \cdot kg^{-1} \cdot h^{-1}$, approximately 6 times as high as that of the unsupported sample. The selectivity for alcohol also increased from 11.5% to 31.4%. Especially, methanol production was remarkably inhibited, and ethanol became the predominant product. The CO_2 was yielded from the water–gas–shift (WGS) side reaction. No significant change in CO_2 production was observed when the Mo/AC weight ratio increased from 30% to 50%.

Table 6 lists the results of the effect of the reduction temperature on the catalytic performance. Increasing the reduction temperature promoted alcohol formation, especially $C_{2+}OH$ selectivity. The optimal reduction temperature was 798 K. Under this condition, the total alcohol STY reached 170.2 $g \cdot kg^{-1} \cdot h^{-1}$ with a selectivity of 42.0%, and the carbon atomic ratio of $MeOH/C_{2+}OH$ decreased to 0.40. The obtained activity results, especially the alcohol STY and $MeOH/C_{2+}OH$ ratio, are very

encouraging because they were tested under very mild conditions of 5.0 MPa and 2400 h^{-1}. With a further increase in the reduction temperature, the catalytic performance decreased. The stability of the K–Co–Mo/AC catalysts with Mo/AC weight ratio of 40% was tested continuously for 100 h under the conditions of 573 K, 5.0 MPa, 3600 h^{-1}. The result was shown in Figure 9. It is clear that after 24 h induction period, the CO conversion and the selectivity for alcohol remained stable, indicating that the catalyst did not show any obvious deactivation after reaction for 100 h.

The properties of the support significantly affect the synthesis of alcohols from syngas. Some acid metal oxide supports such as Al_2O_3 and SiO_2 suppress alcohol formation because their surface acidity is active for alcohol dehydration. Activated carbon supports have some potential advantages such as large surface area, high thermal stability, resistance to acidic or basic media, low tendencies of carbon deposition, and less dehydration. From the BET, XRD, and XAFS results, the used activated carbon support has a large surface area, which facilitates particle distribution and high metal dispersion. The Mo species can even be dispersed as a monolayer on the support surface at a relative low Mo loading (Mo/AC weight ratio of 10%). First, this result suggests that the supported catalyst has a high active surface area, which leads to higher activity compared to the unsupported catalyst. Second, and more importantly, as seen from the nitrogen adsorption–desorption results, the activated carbon support had a large pore volume and mesoporous structure, and the mesoporous structural integrity of the supported catalysts was unchanged after the

impregnation of the catalyst species. The pore size and mesoporosity of the support significantly affected alcohol formation, especially alcohol product distribution, as suggested by Surisetty et al.[19] For the oxidized Mo-based catalyst, the reaction mechanism for producing C_{2+} alcohol is different from that for producing methanol. Methanol is directly formed by the hydrogenation of non-dissociatively adsorbed CO. The formation of higher alcohols is generally thought to occur via a CO insertion mechanism. First, the dissociation of adsorbed CO forms CH_2, followed by the growth of the alkyl chain via CH_2 insertion. Next, the non-dissociatively adsorbed CO insertion to an alkyl group forms an acyl species that can be hydrogenated to the corresponding alcohol or to a longer alkyl group. Hydrocarbons are formed from the hydrogenation of the alkyl group.[20] From the perspective, higher alcohols are secondary products, and the alkyl group serves as the reaction intermediate. Compared to the unsupported catalyst with a very small pore volume and larger pore size, the mesoporous structure of the supported catalyst is suggested to increase the mass diffusion restriction of molecules to some extent. Consequently, the residence time of intermediates in the pore can be prolonged, which is favorable for the formation of higher alcohols. This conclusion is consistent with the results reported by Li et al.[21] They found that for the carbon-supported Mo-based catalyst, increasing the space velocity enhances methanol production while suppressing hydrocarbon and higher alcohol formation because a higher space velocity is associated with a lower residence time, and a lower residence time results in a larger fraction of the primary product and smaller fractions of secondary products. The reduction state of the

surface Mo species also plays an important role for alcohol synthesis. XPS results indicated that on the surface of the supported catalyst, besides Mo^{6+} and Mo^{4+} species, a lower-valence-state $Mo^{\delta+}$ ($1 < \delta < 4$) species was observed. The $Mo^{\delta+}$ ($1 < \delta < 4$) species is regarded as the adsorption site for non-dissociative CO and responsible for alcohol formation.[20] Our previous study based on in situ Diffuse reflectance spectroscopy also confirmed this result.[15] The formation of $Mo^{\delta+}$ ($1 < \delta < 4$) species can promote CO adsorption on the surface and favor alcohol formation. A similar result was obtained by Li et al.[22] They suggested that the Mo species with intermediate-valence state (averaged around +3.5) are more likely to be the active site for alcohol synthesis from CO hydrogenation. The catalytic activity was optimized at a Mo/AC weight ratio of 40% and a reduction temperature of 798 K, which may be attributed to the high content of $Mo^{\delta+}$ species on the surface under these conditions.

4. Conclusion

A type of large surface area and mesoporous activated carbon was used as the support for the K–Co–Mo catalyst prepared by a modified sol–gel method. The active species had a high dispersion on the support surface, and the mesoporous structural integrity of the supported catalyst was unchanged. With an increase in the Mo loading, the surface Mo atoms gradually changed from tetrahedrally coordinated Mo^{6+} species to octahedrally coordinated Mo^{4+}. Increasing the Mo loading can promote the reduction of Mo species. The K–Co–Mo/AC catalyst exhibited a much higher activity for the synthesis of mixed alcohols as compared to the unsupported catalyst.

Especially, the $C_{2+}OH$ content in alcohol distribution significantly increased. The reason can be attributed to the fact that the supported catalyst have a high active surface area, and the mesoporous structure is suggested to prolong the residence time of intermediates for alcohol formation in the pore to some extent, thus favoring the formation of higher alcohols. The surface $Mo^{\delta+}$ ($1 < \delta < 4$) species formed on the reduced catalyst is suggested to be responsible for alcohol synthesis. The high activity of the catalyst with a Mo/AC weight ratio of 40% and a reduction temperature of 798 K may be attributed to the high content of $Mo^{\delta+}$ ($1 < \delta < 4$) species on the surface.

Acknowledgments

This study was supported by the National Nature Science Foundation of China (11179034, 11205159), National Basic Research Program of China (973 Program, 2012CB922004).

Notes and references

1 (a) V. Subramani and S. K. Gangwal. *Energy & Fuels* 2008, **22**, 814; (b) M. Gupta, M. L. Smith and J. J. Spivey. *ACS Catal.,* 2011, **1**, 641; (c) Y. Z. Fang, Y. Liu and L. H. Zhang. *Appl. Catal., A,* 2011, **397**, 183; (d) V. R. Surisetty, Y. Hu, A. K. Dalai and J. Kozinski, *Appl. Catal., A,* 2011, **392**, 166; (e) V. M. Lebarbier, D. Mei, D. H. Kim, A. Andersen, J. L. Male, J. E. Holladay, R. Rousseau and Y. Wang, *J. Phys. Chem. C,* 2011, **115**, 17440; (f) T. Toyoda, T. Minami and E. W. Qian. *Energy Fuels,* 2013, **27**, 3769; (g) V. Mahdavi, M. H. Peyrovi, M. Islami and J. Y. Mehr, *Appl. Catal., A,*

2005, **281**, 25.

2 (a) T. Tatsumi, A. Muramatsu, T. Fukunaga and H. O. Tominaga, *Polyhedron,* 1986, **5**, 257; (b) V. R. Surisetty, A. Tavasoli and A. K. Dalai, *Appl. Catal., A*, 2009, **365**, 243; (c) J. M. Christensen, P. A. Jensen and A. D. Jensen, *Ind. Eng. Chem. Res.,* 2011, **50**, 7949; (d) H. Shou, D. Ferrari, D. G. Barton, C. W. Jones and R. J. Davis, *ACS Catal.,* 2012**, 2**, 1408; (e) S. F. Zaman and K. J. Smith, *Appl. Catal., A,* 2010, **378**, 59; (f) J. Iranmahboob, H. Toghiani, D. O. Hill, F. Nadim, *Fuel Process. Technol.,* 2002, **79**, 71; (g) S. Zaman and K. J. Smith, *Catal. Rev. - Sci. Eng.,* 2012, **54**, 41.

3 (a) Y. C. Xie, B. M. Naasz and G. A. Somorjai, *Appl. Catal.,* 1986, **27**, 233; (b) J. Iranmahboob, H. Toghiani and D. O. Hill, *Appl. Catal., A,* 2003, **247**, 207; (c) T. Tatsumi, A. Muramatsu and H.-o. Tominaga, *Appl. Catal., A,* 1986, **27**, 69.

4 M. Xiang and J. Zou. *J. Catal.,* 2013, **2013**, 1.

5 (a) Z. R. Li. *Catal. Lett.,* 2000, **65**, 43; (b) Y. L. Fu, Z. R. Li and M. Jiang, *Appl. Catal., A*, 1999, **187**, 187; (c) T. Toyoda and E. W. Qian, *J. Jpn. Petrol. Inst.,* 2014, **57**, 171; (d) D. Li, N. Zhao, H. Qi, W. Li, Y. H. Sun and B. Zhong, *Catal. Commun.,* 2005, **6**, 674.

6 V. R. Surisetty, A. K. Dalai and J. Kozinski, *Appl. Catal., A,* 2010**, 385**, 153.

7 Z. R. Li, Y. L. Fu, J. Bao, M. Jiang, T. D. Hu, T. Liu and Y. N. Xie, *Appl. Catal., A,* 2001, **220**, 21.

8 (a) D. A. Storm, *Top. Catal.,* 1995, **2**, 91; (b) K. Fujimoto and T. Oba, *Appl. Catal.,* 1985, **13**, 289.

9 Z. Y. Liu, X. G. Li, M. R. Close, E. L. Kugler, J. L. Petersen and D. B. Dadyburjor, *Ind. Eng. Chem. Res.,* 1997, **36**, 3085.

10 (a) V. R. Surisetty, I. Eswaramoorthi and A. K. Dalai. *Fuel,* 2012, **96**, 77; (b) H. Okatsu, M. R. Morrill, H. Shou, D. G. Barton, D. Ferrari, R. J. Davis, P. K. Agrawal and C. W. Jones, *Catal. Lett.,* 2014, **144**, 825; (c) M. R. Morrill, N. T. Thao, H. Shou, R. J. Davis, D. G. Barton, D. Ferrari, P. K. Agrawal and C. W. Jones, *ACS Catal.,* 2013, **3**, 1665.

11 (a) Y. A. Ryndin, R. F. Hicks, A. T. Bell and Y. I. Yermakov, *J. Catal.,* 1981, **70**, 287; (b) G. Z. Bian, L. Fan, Y. L. Fu and K. Fujimoto, *Ind. Eng. Chem. Res.,* 1998, **37**, 1736.

12 J. C. Duchet, E. M. Vanoers, V. H. J. Debeer and R. Prins, *J. Catal.,* 1983, **80**, 386.

13 (a) F. Rodríguez-reinoso, *Carbon,* 1998, **36**, 159; (b) B. E. Concha, G. L. Bartholomew and C. H. Bartholomew, *J. Catal.,* 1984, **89**, 536.

14 J. Bao, Z. Liu, Y. Zhang and N. Tsubaki, *Catal. Commun.,* 2008, **9**, 913.

15 M. M. Zhang, W. Zhang, W. Xie, Z. M. Qi, G. M. Wu, M. M. Lv, S. Sun and J. Bao. *J. Mol. Catal. A: Chem.,* 2014, **395**, 269.

16 J. Rouquerol, D. Avnir, C. W. Fairbridge, D. H. Everett, J. M. Haynes, N. Pernicone, J. D. F. Ramsay, K. S. W. Sing and K. K. Unger, *Pure Appl. Chem.,* 1994, **66**, 1739.

17 D. O. Scanlon, G. W. Watson, D. J. Payne, G. R. Atkinson, R. G. Egdell and D. S. L. Law, *J. Phys. Chem. C,* 2010, **114**, 4636.

18 J.-G. Choi and L. T. Thompson, *Appl. Surf. Sci.,* 1996, **93**, 143.

19 V. R. Surisetty, A. K. Dalai and J. Kozinski, *Appl. Catal., A,* 2011, **393**, 50.

20 A. Muramatsu, T. Tatsumi and H. Tominaga, J. *Phys. Chem. C*, 1992, 96, 1335.

21 X. G. Li, L. J. Feng, Z. Y. Liu, B. Zhong, D. B. Dadyburjor and E. L. Kugler, *Ind. Eng. Chem. Res.,* 1998, **37**, 3853.

22 X. G. Li, L. J. Feng, L. J. Zhang, D. B. Dadyburjor and E. L. Kugler, *Molecules,* 2003, **8**, 13.

Table Captions

Table 1

Textural properties of the pure support and the supported and unsupported K–Co–Mo catalysts.

Table 2

XPS data of Mo 3d for the fresh K–Co–Mo/AC catalysts.

Table 3

XPS data of Mo 3d for the K–Co–Mo/AC catalysts reduced at 773 K.

Table 4

Distribution of Mo species for the K–Co–Mo/AC catalysts with a Mo/AC weight ratio of 40% at different reduction temperatures.

Table 5

Effect of Mo loading on the catalytic performance toward alcohol formation from syngas.

Table 6

Effect of reduction temperature on the catalytic performance toward alcohol formation from syngas.

Figure Captions

Figure 1

XRD patterns of (a) activated carbon; fresh K–Co–Mo/AC catalysts at different Mo/AC weight ratios of (b) 10%; (c) 30%; (d) 40%; (e) 50%; (f) unsupported K–Co–Mo catalyst.

Figure 2

XRD patterns of reduced K–Co–Mo/AC catalysts at different Mo/AC weight ratios of (a) 10%; (b) 30%; (c) 40%; (d) 50%. Reduction temperature: 773 K.

Figure 3

Nitrogen adsorption–desorption isotherms of (a) activated carbon; K–Co–Mo/AC catalysts at different Mo/AC weight ratios of (b) 10%; (c) 30%; (d) 40%; (e) 50%; (f) unsupported K–Co–Mo catalyst.

Figure 4

Mo K-edge XANES spectra of (a) standard MoO_3; (b) standard MoO_2; fresh K–Co–Mo/AC catalysts at different Mo/AC weight ratios of (c) 10%; (d) 30%; (e) 50%; (f) unsupported K–Co–Mo catalyst.

Figure 5

Fourier transforms of Mo K-edge EXAFS of fresh K–Co–Mo/AC catalysts at different Mo/AC weight ratios of (a) 10%; (b) 30%; (c) 50%; (d) unsupported K–Co–Mo catalyst; (e) standard MoO_3; (f) standard MoO_2.

Figure 6

XPS spectra of Mo 3d for fresh K–Co–Mo/AC catalysts at different Mo/AC weight ratios of (a) 10%; (b) 30%; (c) 40%; (d) 50%.

Figure 7

XPS spectra of Mo 3d for reduced K–Co–Mo/AC catalysts at different Mo/AC weight ratios of (a) 10%; (b) 30%; (c) 40%; (d) 50%. Reduction temperature: 773 K.

Figure 8

XPS spectra of Mo 3d of the K–Co–Mo/AC catalysts at a Mo/AC weight ratio of 40% reduced at (a) 723 K; (b) 748 K; (c) 773 K; (d) 798 K; (e) 823 K.

Figure 9

Stability test of K-Co-Mo/AC catalyst with Mo loading of 40wt% at 573 K, 5.0 MPa and 3600 h^{-1}.

Table 1

Mo/AC (wt%)	BET surface area (m^2/g)	Total pore volume (cm^3/g)	Average pore diameter (nm)
0	872.59	0.46	4.70
10%	670.59	0.34	4.70
30%	402.83	0.21	5.32
40%	474.78	0.24	5.22
50%	323.78	0.17	9.67
K–Co–Mo	21.22	0.07	24.93

Table 2

Mo/AC (wt%)	Mo^{6+}			Mo^{4+}		
	$3d_{5/2}$ (eV)	$3d_{3/2}$ (eV)	Percentage (%)	$3d_{5/2}$ (eV)	$3d_{3/2}$ (eV)	Percentage (%)
10%	232.5	235.6	100	-	-	-
30%	232.6	235.8	96.24	230.8	234.0	3.76
40%	232.6	235.8	92.58	230.8	234.0	7.42
50%	232.6	235.8	91.50	230.8	234.0	8.50

Table 3

Mo/AC (wt%)	Mo^{6+}			Mo^{4+}			$Mo^{\delta+}$		
	$3d_{5/2}$ (eV)	$3d_{3/2}$ (eV)	Percentage (%)	$3d_{5/2}$ (eV)	$3d_{3/2}$ (eV)	Percentage (%)	$3d_{5/2}$ (eV)	$3d_{3/2}$ (eV)	Percentage (%)
10%	232.3	235.4	52.60	230.5	233.7	36.35	229.4	232.6	11.05
30%	232.3	235.4	49.76	230.5	233.7	37.24	229.4	232.6	13.50
40%	232.3	235.4	46.84	230.5	233.7	34.31	229.4	232.6	18.85
50%	232.3	235.4	42.38	230.5	233.7	41.28	229.4	232.6	16.33

Table 4

Reduction Temperature (K)	Mo^{6+} (%)	Mo^{4+} (%)	$Mo^{\delta+}$ (%)
723	62.49	28.65	8.86
748	47.34	38.26	14.40
773	46.84	34.31	18.85
798	50.76	28.64	20.60
823	52.78	27.63	19.60

Table 5

Mo/AC (wt%)	CO Conv. (C %) to		Alc. Sel. [a]	Alc. STY	C_nOH Sel. (C%)				MeOH/ $C_{2+}OH$
	ROH+HC	CO_2	(C %)	($g \cdot Kg^{-1} \cdot h^{-1}$)	MeOH	EtOH	PrOH	BuOH	
10%	15.70	9.84	22.20	65.51	11.47	7.74	5.81	0.44	1.07
30%	26.38	21.01	28.13	106.68	10.52	10.44	5.81	1.36	0.60
40%	27.32	20.01	31.43	126.18	10.97	11.74	6.89	1.83	0.54
50%	31.63	23.04	21.27	110.47	7.82	7.76	4.51	1.19	0.58
K–Co–Mo	20.74	17.48	11.51	21.10	5.00	3.91	2.07	0.53	0.78

[a] based on CO_2-free carbon atoms.

Reaction conditions: T = 573 K; P = 5.0 MPa; GHSV = 2400 h^{-1}; $H_2/CO = 2$.

Table 6

T (K)	CO Conv. (C %) to		Alc. Sel. [a] (C %)	Alc. STY ($g \cdot Kg^{-1} \cdot h^{-1}$)	C_nOH Sel. (C%)				MeOH/ $C_{2+}OH$
	ROH+HC	CO_2			MeOH	EtOH	PrOH	BuOH	
723	20.18	14.67	21.64	87.14	8.23	8.13	4.26	1.02	0.61
748	24.61	21.57	22.26	96.99	7.79	8.49	4.74	1.25	0.54
773	27.32	20.01	31.43	126.18	10.97	11.74	6.89	1.83	0.54
798	26.04	21.13	42.05	170.24	12.08	16.77	10.07	3.14	0.40
823	28.15	24.07	32.55	143.34	8.44	13.30	7.68	3.09	0.35

[a] based on CO_2-free carbon atoms.

Reaction conditions: T = 573 K; P = 5.0 MPa; GHSV = 2400 h^{-1}; $H_2/CO = 2$.

Figure 1

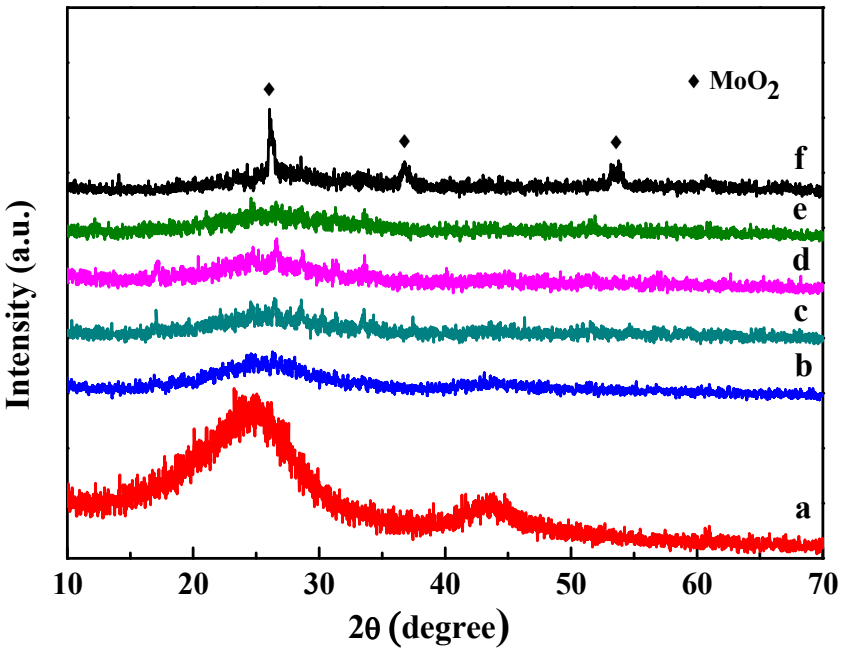

Figure 2

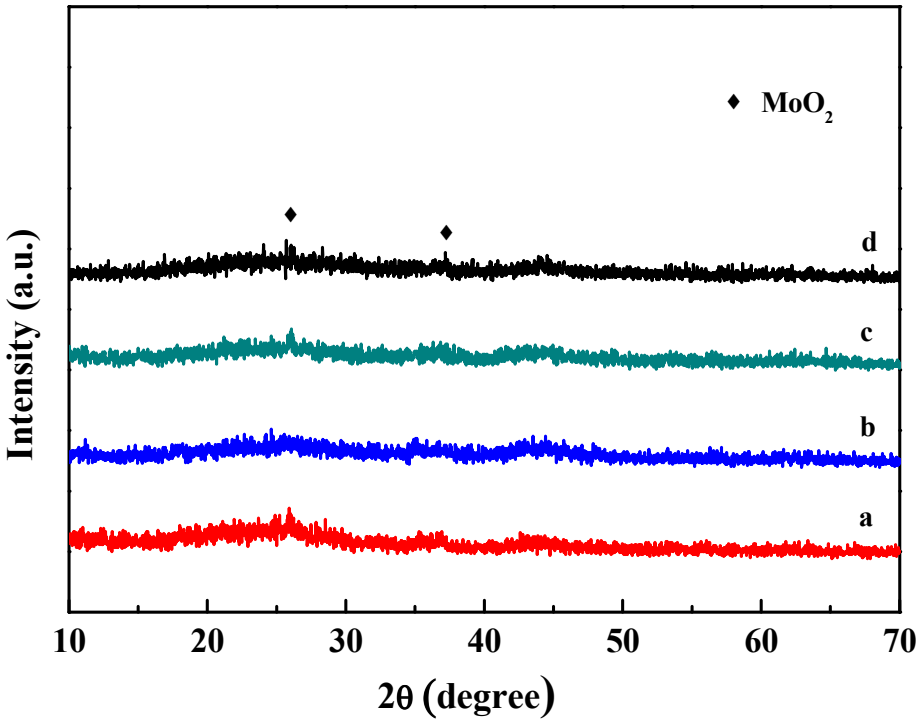

Figure 3

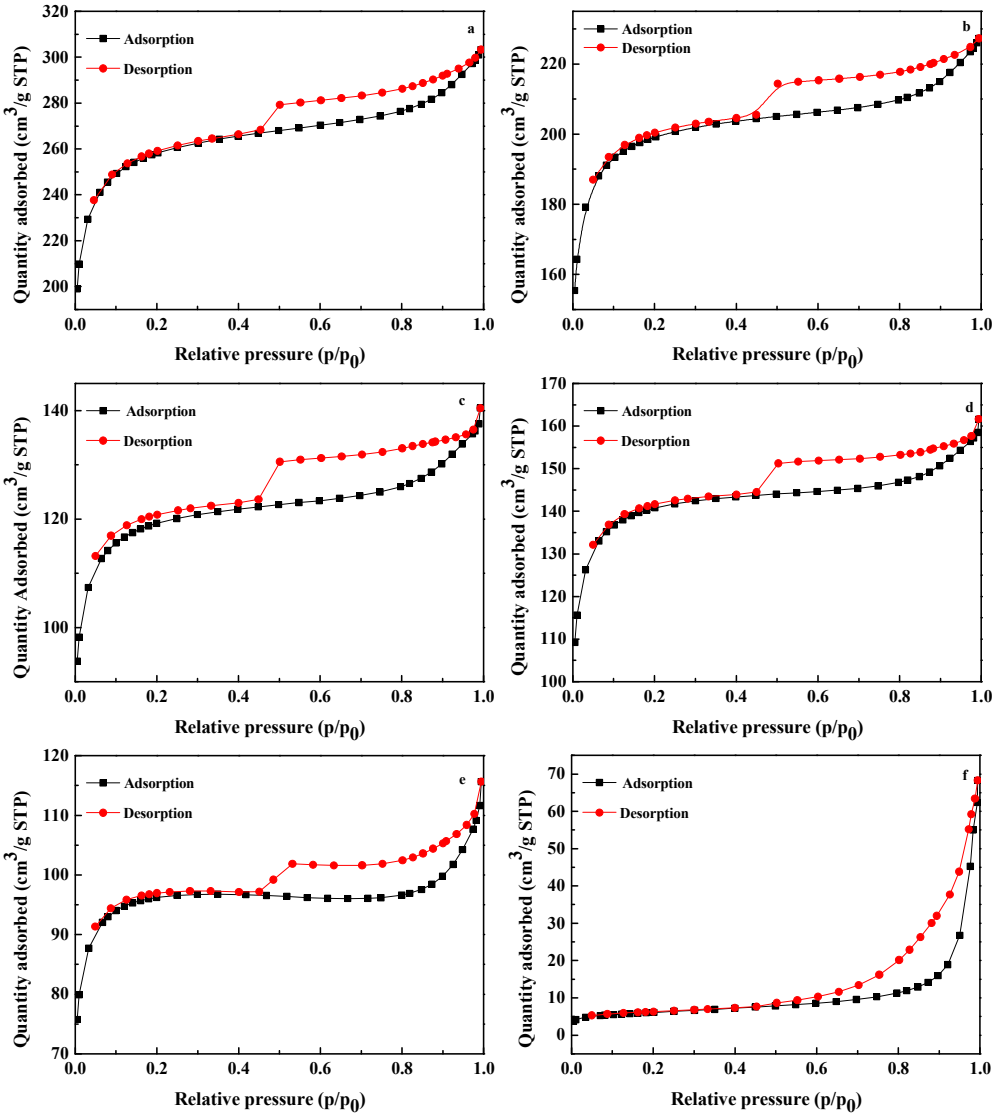

Figure 4

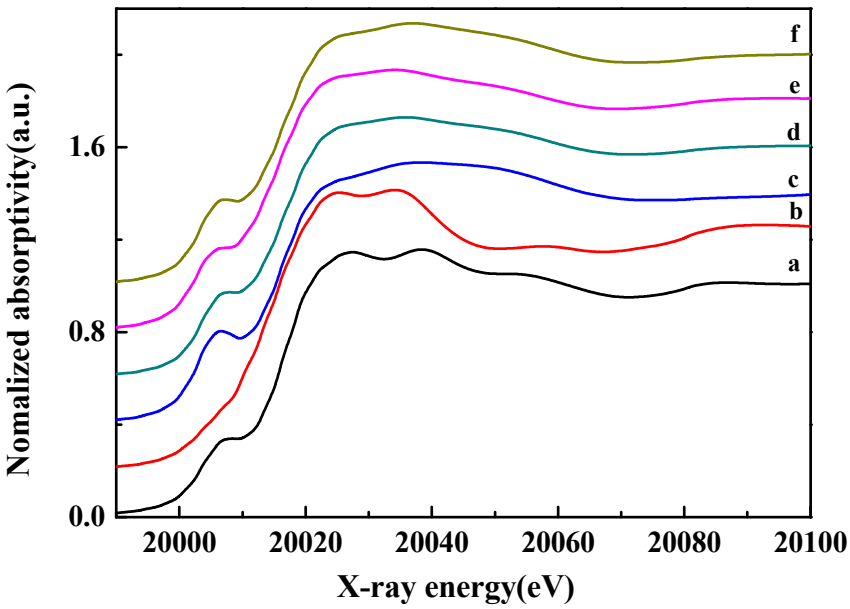

Figure 5

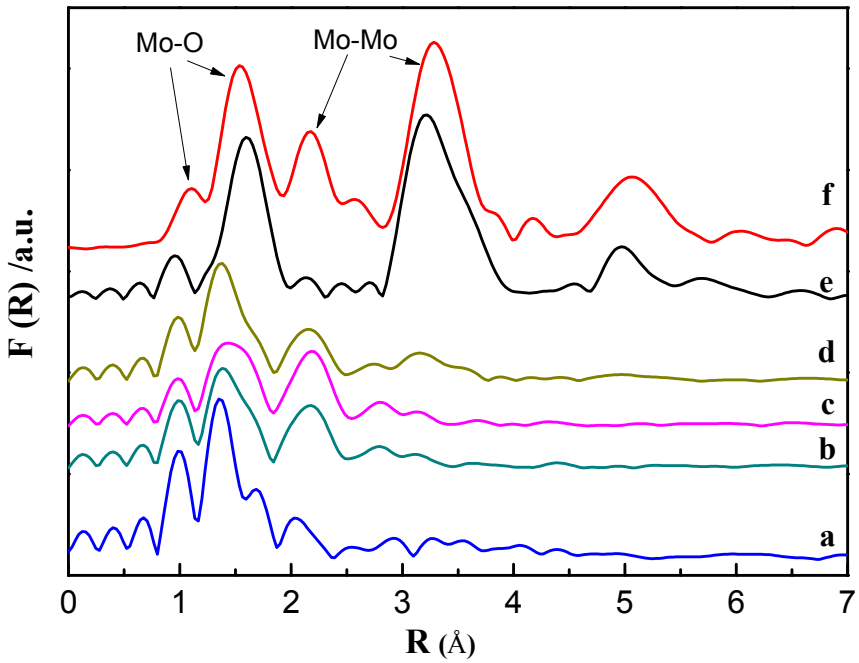

Figure 6

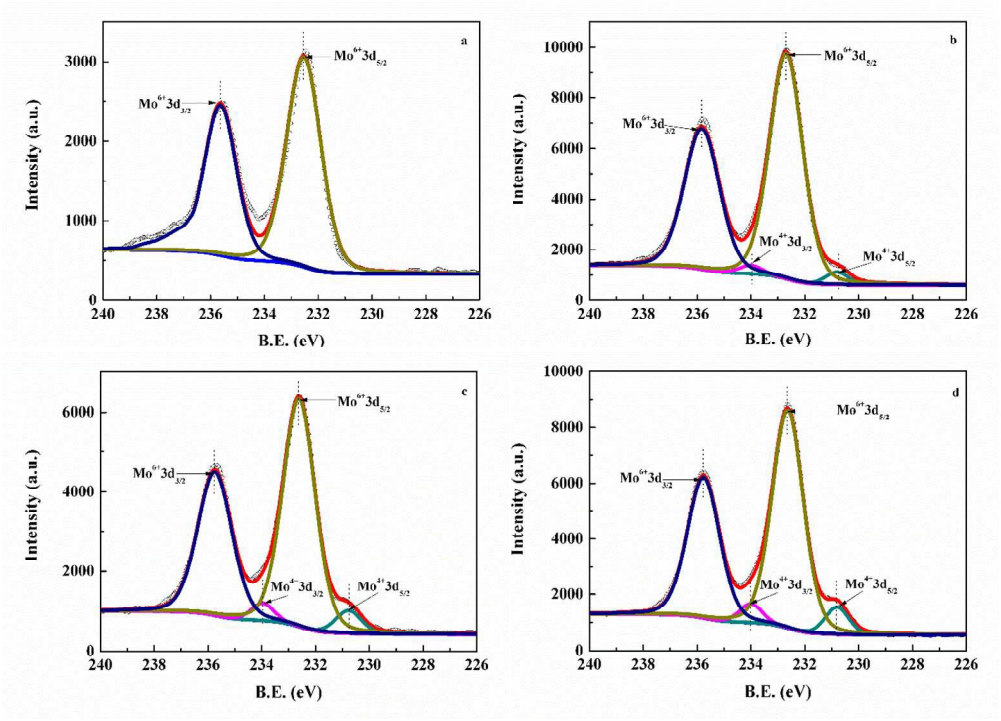

Figure 7

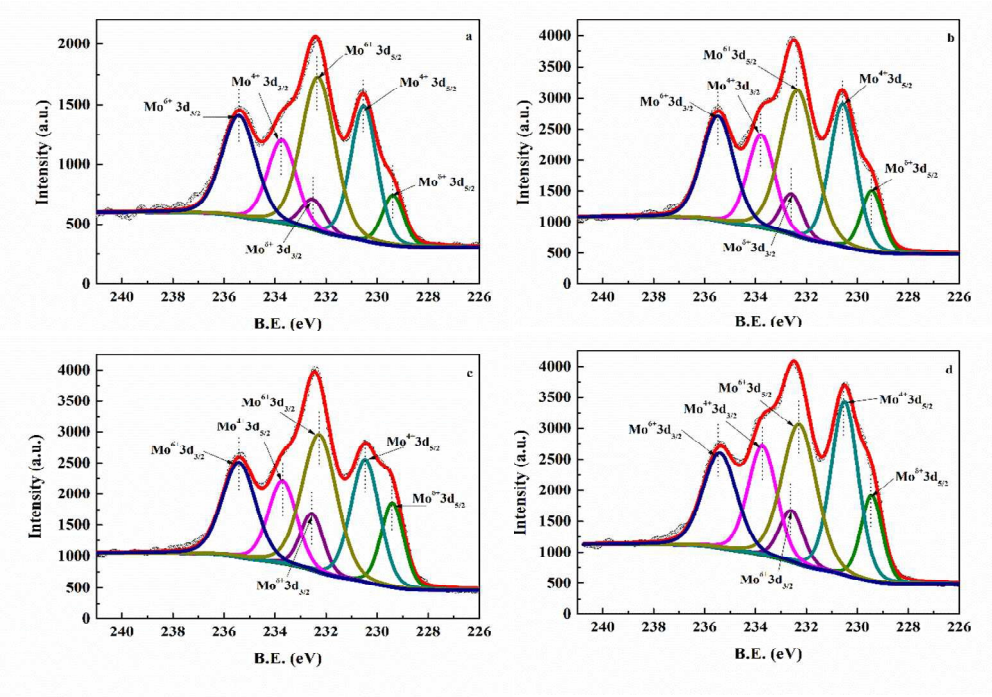

Figure 8

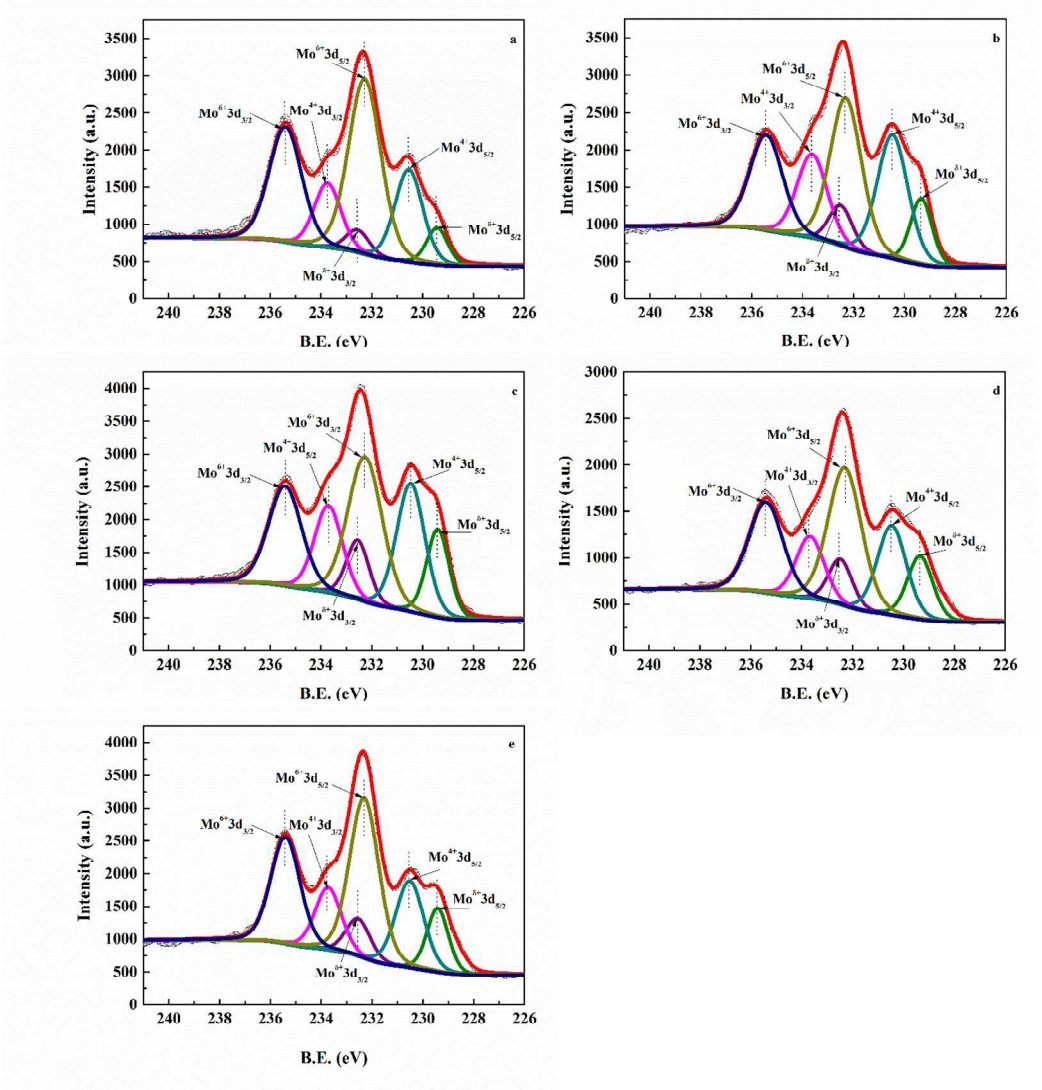

Figure 9